Published on 16 April 2015. Downloaded by Bilkent University on 05/05/2015 13:53:39.

PCCP

ROYAL SOCIETY OF CHEMISTRY

PAPER

View Article Online
View Journal

Cite this: DOI: 10.1039/c5cp00414d

Realization of a p–n junction in a single layer boron-phosphide

Deniz Çakır,*[a] Deniz Kecik,[b] Hasan Sahin,[a] Engin Durgun[b] and Francois M. Peeters[a]

Two-dimensional (2D) materials have attracted growing interest due to their potential use in the next generation of nanoelectronic and optoelectronic applications. On the basis of first-principles calculations based on density functional theory, we first investigate the electronic and mechanical properties of single layer boron phosphide (h-BP). Our calculations show that h-BP is a mechanically stable 2D material with a direct band gap of 0.9 eV at the *K*-point, promising for both electronic and optoelectronic applications. We next investigate the electron transport properties of a p–n junction constructed from single layer boron phosphide (h-BP) using the non-equilibrium Green's function formalism. The n- and p-type doping of BP are achieved by substitutional doping of B with C and P with Si, respectively. C(Si) substitutional doping creates donor (acceptor) states close to the conduction (valence) band edge of BP, which are essential to construct an efficient p–n junction. By modifying the structure and doping concentration, it is possible to tune the electronic and transport properties of the p–n junction which exhibits not only diode characteristics with a large current rectification but also negative differential resistance (NDR). The degree of NDR can be easily tuned *via* device engineering.

Received 22nd January 2015,
Accepted 13th April 2015

DOI: 10.1039/c5cp00414d

www.rsc.org/pccp

1 Introduction

Major improvements in the capabilities of electronics have been achieved by the increasing use of silicon-based devices for half a century. However, the current silicon technology is predicted to reach its limits in the near future. A family of materials with reduced dimension and size, in particular III–V binary compound semiconductors, has gained importance. Recent advances in the growth of graphene and graphene like ultra-thin materials have not only enabled the preparation of high quality ultra-thin films but also provided researchers with a variety of single layer crystals with remarkable electronic properties at the nanoscale.

Following the synthesis of graphene,[1–4] single layer hexagonal boron nitride (h-BN) has attracted considerable interest during the past ten years. SiO_2 substrates which have been widely used as supporting materials for ultra-thin monolayer crystals are known to degrade the charge carrier mobility of the overlying systems due to the existing defect states.[5–8] On the other hand, its clean monolayer hexagonal crystal structure, flatness and dielectric behavior ($\varepsilon \cong 3$–4) make h-BN an ideal choice as a substrate for nanoscale transistors. In addition, h-BN has already been used in various applications such as protective coatings,[9,10] transparent membranes[7] and deep ultraviolet lasers.[11] A majority of the studies conducted so far have been limited to metal growth on supported h-BN,[12,13] energetics of various defects,[14,15] substrate induced nanomesh formation[16] and characteristics of various vacancy types.[17,18] In addition, Park *et al.*[19] showed that carbon doped monolayer h-BN has unique magnetic and optical properties with several possible applications in magneto-optics and opto-electronics.[19]

Among the III–V binary compounds boron phosphide (BP) has also attracted considerable attention. Although BP is abundant in nature in the zincblende phase, it can also be found in rocksalt and β-Sn phases.[20,21] Moreover, the synthesis of cubic BP *via* a benzene-thermal reaction of boron powder and phosphorus trichloride with metallic lithium or sodium was achieved by Gu *et al.*[22] In addition to bulk BP, recent studies have revealed the importance of nanostructured BP for technological applications. Synthesis of nanosized BP structures and the demonstration of BP-based electrodes for sensitized liquid junction photovoltaic solar cells were reported by Schroten *et al.*[23] Stability, functionalization and various applications of BP nanotubes (NTs) were also studied.[24,25] It was also shown that Si doping in single walled BPNTs results in a reduction of the electronic band gap and an increase of electrical conductance.[26] Moreover, Sahin *et al.* predicted the stability of monolayer boron phosphide with hexagonal crystal symmetry (h-BP).[27] Dong and coworkers recently predicted that boron phosphide and silicon carbide nanoribbons can be used in the fabrication of promising nanoelectronic and spintronic devices.[28]

[a] *Department of Physics, University of Antwerp, Groenenborgerlaan 171, 2020 Antwerpen, Belgium. E-mail: deniz.cakir@uantwerpen.be*
[b] *UNAM-National Nanotechnology Research Center, Bilkent University, Ankara 06800, Turkey*

Published on 16 April 2015. Downloaded by Bilkent University on 05/05/2015 13:53:39.

Motivated by recent experiments demonstrating the successful synthesis of monolayers of III–V binary compounds[29,30] and theoretical work[27] reporting the stability of such materials, we investigated the electronic and transport properties of doped h-BP, by firstly examining the mechanical stability of the pristine structure. Furthermore, we propose the utilization of h-BP for the construction of a p–n junction.

This paper is organized as follows: details of the computational methodology are given in Section 2, electronic properties and mechanical stability of pristine and doped h-BP are presented in Section 3 and electronic transport properties through p- and n-doped h-BP are examined in Section 4. Conclusions drawn from this work are given in Section 5.

2 Computational methodology

First-principles calculations were performed using the plane-wave pseudopotential Vienna ab initio simulation package (VASP).[31,32] We have employed the generalized gradient approximation (GGA) within the projector-augmented wave method (PAW)[33] where the exchange–correlation functional is approximated with the PBE functional[34] using a plane-wave energy cutoff of 500 eV. Since the band gaps are underestimated at the DFT-GGA level, we also carried out calculations using the HSE06 hybrid functional.[35–37] A K-point sampling of $11 \times 11 \times 1$ was used for the 5×5 supercell. All structures were relaxed using the special Davidson algorithm[38] with simultaneous minimization of the total energy and the interatomic forces. The convergence for the total energy was set to 10^{-5} eV and the maximum residual force allowed on each atom was fixed at 10^{-2} eV Å^{-1}. The phonon dispersion curves are calculated using the PHON[39] package implemented in VASP.

Electronic transport across the p–n junction was calculated using the self-consistent non-equilibrium Green function (NEGF) technique as implemented in TranSIESTA[40] which is interfaced using the SIESTA code.[41] Double-zeta (plus polarization) numerical orbital basis sets were used for all atoms. We employed norm-conserving pseudopotentials[42] (the PBE functional) and an energy cutoff for the real-space mesh of 250 Ry. In order to obtain an accurate transmission spectrum and electron current as a function of applied bias, the Brillouin zone normal to the transport direction (which is the z-direction in this study) was sampled using the k-mesh of 71×1. In our transport calculations, depending on the doping concentration and device geometry, the sizes of the rectangular electrodes are 11.13 and 16.06 Å. Similarly, the corresponding total cell sizes including electrodes in the transport calculations along the transport or z direction are set to at least 44 Å. For the longest device geometry, the total cell size is found to be 65 Å. The vacuum space normal to the z direction is 12 Å.

While the SIESTA code uses a localized basis set and norm-conserving pseudopotentials, the calculated lattice parameters for the undoped BP monolayer agree very well with those obtained from the VASP code. For instance, the lattice parameter for the single layer BP is found to be 3.21 Å using VASP and 3.26 Å using SIESTA. Similarly, the band gap of undoped BP is calculated to be 0.91 eV using VASP and 0.97 eV using SIESTA.

3 Stability and the electronic structure of monolayer boron-phosphide

3.1 Mechanical stability of single layer pristine BP

Before discussing the possible implementation of BP in the p–n junction applications, we first present its stability and electronic properties. Since single layer BP has not been synthesized yet, it is mandatory to investigate its stability as a 2D material. For this reason, we present a detailed study of the mechanical and vibrational properties of pristine BP.

In order to investigate the stability of single layer BP, analysis of the phonon modes provides a reliable test. In Fig. 1, we present the calculated dispersion of the phonon modes of monolayer BP. Our calculations show that the phonon spectrum of BP yields no imaginary frequencies, which is the signature of instability. As is clear from Fig. 1, except for the lowest acoustic branch, which is quadratic since transversal forces decay rapidly, longitudinal and transverse acoustic modes are linear for $\mathbf{k} \rightarrow 0$. While the first three phonon branches belong to the flexural mode (ZA), transversal acoustic (TA) and longitudinal acoustic (LA) modes have zero frequency at the zone center and the lowest energy optical branches which belong to the well-known ZO phonon mode appear at 299 cm^{-1}. This mode, similar to the A_{1g} mode in graphene, has out-of-plane counter-phase characteristics. In addition, the degenerate high-frequency mode at 956 cm^{-1} is composed of longitudinal and transverse optical phonon branches. Eigenvector analysis reveals that LO and TO modes have E_g characteristics that corresponds to in-plane counter-phase motions of neighboring atoms. Therefore, as a characteristic property of the monolayer BP structure, one can expect two main peaks at 299 and 956 cm^{-1}, in Raman intensity measurements. The calculated phonon dispersion and values of the vibrational eigenfrequencies are in good agreement with the values reported in ref. 27. It is seen that only the highest optical mode has a slightly lower eigenfrequency than that reported in ref. 27. Here the reason

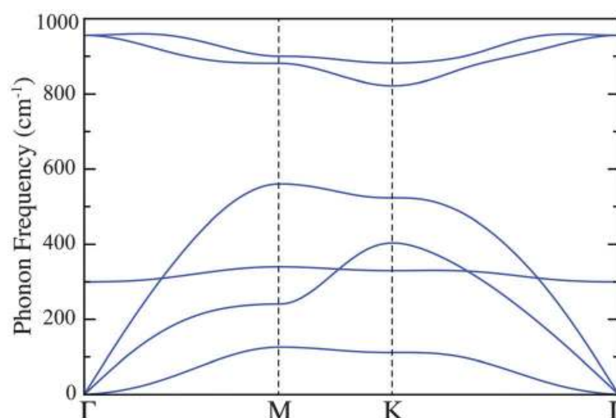

Fig. 1 Phonon dispersion curve of single layer BP.

This journal is © the Owner Societies 2015

View Article Online

Table 1 Calculated elastic constants (in units of N m^{-1}), young modulus Y (in units of N m^{-1}), and Poisson's ratio ν

	C_{11}	C_{12}	Y	ν
MoS_2	132.7	33.0	124.5	0.25
Graphene	351.9	61.8	341.0	0.18
BN	290.2	64.4	275.9	0.22
BP	145.9	38.8	135.6	0.27

for the slight deviation is the overestimated bond strength and phonon frequencies in the LDA approach in ref. 27.

For better perception of the mechanical stability, the elastic constants of single layer BP are also calculated. Since single layer BP belongs to the D_{3h} space group, there are two independent elastic constants, namely, C_{11} and C_{12}. The in-plane Young's modulus (Y) and Poisson's ratio (ν) can be directly obtained from the following relationships: $Y = (C_{11}{}^2 - C_{12}{}^2)/C_{11}$ and $\nu = C_{12}/C_{11}$. The calculated C_{11}, C_{12}, Y, and ν values are 145.9 N m^{-1}, 38.8 N m^{-1}, 135.6 N m^{-1}, and 0.27, respectively. Comparison with other well known 2D materials, namely graphene, BN, and MoS_2, reveals that BP is mechanically as stable as MoS_2, yet less stiffer than both graphene and single layer h-BN,[27,43] as summarized in Table 1.

3.2 Band structure of single layer pristine BP

The band structure of monolayer BP, which reveals a direct (PBE) band gap of 0.91 eV at the K-point, is displayed in Fig. 2. When calculated with the HSE06 hybrid functional the band gap increases to 1.34 eV. In ref. 27, the energy band gap of monolayer BP was reported to be 0.82 eV (using LDA) and 1.81 eV (using GW). Similarly, a direct band gap of 0.87 eV was predicted by using PBE in ref. 28. In contrast to single-layer, bulk zinc-blende BP is an indirect band gap semiconductor. The experimentally measured[44] and the calculated band gap using *ab initio* methods is 2.02 eV.[45] Once the dimension is reduced from 3D to 2D, not only the band gap is decreased but BP is also converted into a direct gap semiconductor.

It should be noted that monolayer BN, another material within the same class, is an insulator with a large band gap of 4.6 eV.[46] The lower band gap of BP is no surprise and is associated with the different ionicities of each compound, which is also valid for monolayer BAs. This trend was shown earlier for their bulk counterparts,[47,48] and is generalized here to their corresponding monolayer systems. Being a direct band gap semiconductor with both the valence band maximum (VBM) and the conduction band minimum (CBM) located at the K-point, BP turns out to be a suitable 2D semiconductor for nanoelectronic applications, with a tunable band gap by chemical doping, as was previously shown for bulk BP.[48]

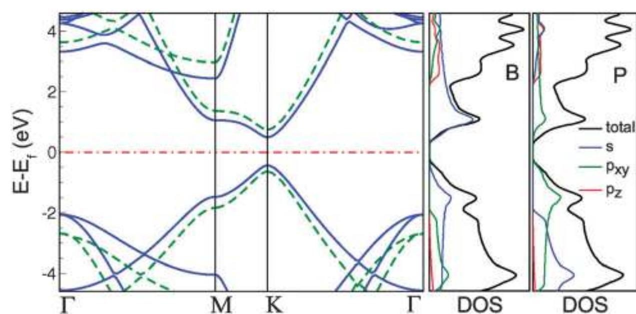

Fig. 2 Left panel: the band structure of pristine monolayer BP along the high symmetry points of the hexagonal BZ, computed by DFT-GGA (blue lines) and HSE06 (green dashed lines). The Fermi level is set to 0 eV and denoted by red dashed line. Right panels: partial densities of states of B and P atoms computed by DFT-GGA.

For better visualization, decomposed DOS owing to s and p states is magnified with a factor of two.

Effective mass (m^*) is also an important parameter which is indicative of the transport properties of a semiconductor. Here, m^* is calculated as the inverse of the second derivative of $E(\mathbf{k})$ with respect to $\mathbf{k}$. At the VBM, the lateral hole effective mass ($m_h{}^*$) is found to be 0.115 m_0 (along K–Γ) and 0.138 m_0 (along K–M) and at the CBM the lateral electron effective mass ($m_e{}^*$) is 0.120 m_0 (along K–Γ) and 0.151 m_0 (along K–M), where m_0 is the free electron mass. Our results indicate that m^* is nearly isotropic for electrons and holes. When compared with the corresponding 3D systems, $m_e{}^*$ and $m_h{}^*$ are significantly smaller than both the bulk BP counterpart[45] ($m_e{}^*$ (lateral) = 1.216 m_0, $m_e{}^*$ (transverse) = 0.255 m_0, $m_h{}^*$ (heavy hole) = 0.316–0.593 m_0 and $m_h{}^*$ (light hole) = 0.132–0.243 m_0), bulk BN[49] ($m_e{}^*$ (in-plane) = 0.50 m_0, $m_e{}^*$ (out-of-plane) = 1.33 m_0 and $m_h{}^*$ (in-plane) = 0.26 m_0, $m_h{}^*$ (out-of-plane) = 2.21 m_0), and also crystalline Si ($m_e{}^*$ = 0.26 m_0 and $m_h{}^*$ = 0.29 m_0). It is informative to make a similar comparison for the corresponding monolayer semiconducting systems. The calculated m^* values are once again significantly smaller than those of layered BN[50] ($m_e{}^* = m_h{}^* = 0.54$ m_0) and monolayer MoS_2[51] ($m_e{}^*$ = 0.37–0.38 m_0 and $m_h{}^*$ = 0.44–0.48 m_0) and comparable with those of single layer black phosphorus[52] ($m_e{}^*$ = 0.09–0.17 m_0 and $m_h{}^*$ = 0.14–0.22 m_0). These data suggest that monolayer BP is a promising candidate material for the next generation of electronic devices.

3.3 Effect of doping on the electronic properties of single layer BP

A major requirement of a good candidate material for a p–n junction is the presence of shallow p- and n-type doping levels. In other words, the aim is to create donor and acceptor states close enough to the valence and conduction bands, forming impurity bands with reasonable dispersion. In that sense, we chose C-doping which replaces B, and similarly Si for P;[53] due to their proximate atomic numbers to each other. This selection serve as a prototype model to realize p- and n-doped systems. Since boron has three valence electrons, when it is doped with carbon having four valence electrons, n-type doping occurs due to the extra electron. On the other hand, when a silicon atom with four valence electrons replaces one phosphorus atom, p-type doping is achieved due to the missing electron of P. Even though a whole evolution of structural and electronic properties and charge analyses of BP for different system sizes were made we will not repeat it here. We tested regarding the electronic properties of supercells of BP starting from 3 × 3 up to 8 × 8 equivalent to a doping concentration range of 6% to

Published on 16 April 2015. Downloaded by Bilkent University on 05/05/2015 13:53:39.

Published on 16 April 2015. Downloaded by Bilkent University on 05/05/2015 13:53:39.

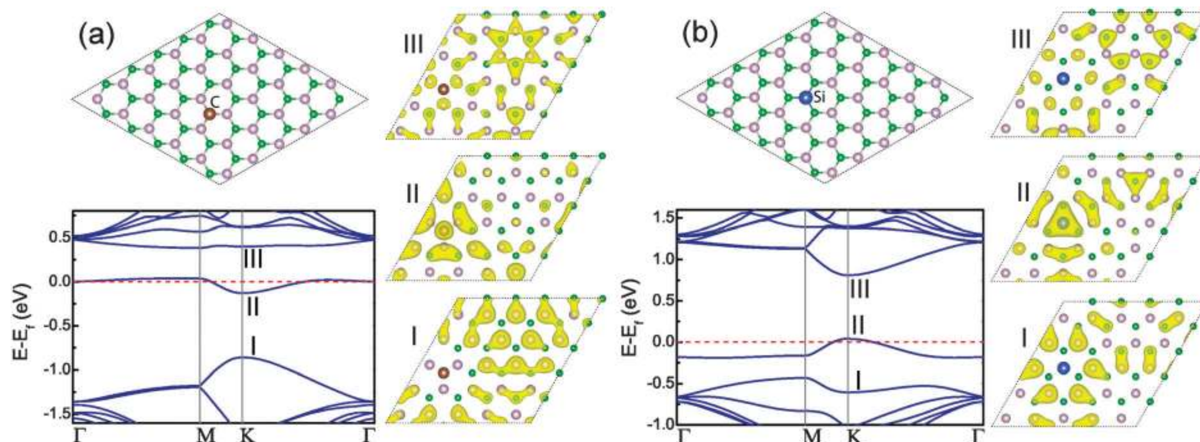

Fig. 3 Electronic structure of (a) C doped and (b) Si doped 5 × 5 supercells of BP along the high symmetry points of the hexagonal BZ. Red dashed line denotes the Fermi level. Right-hand sides of both band structures display the evolution of the partial charge density distributions decomposed over the bands. (I), (II) and (III) denote the top-most valence band, the impurity band, and bottom-most conduction bands, as also indicated in the band plots. Top views of substitutionally doped hexagonal monolayer BP are also shown. The pink, green, brown and blue balls represent the phosphorus, boron, carbon and silicon atoms, respectively.

0.8%. Even if it is a heavily doped system, owing to its 2% doping concentration, a 5 × 5 supercell of BP is considered as a prototype system for p–n junction design, as the impurity band profile is already evident at this size as shown in Fig. 3.

The required substitutional energy, E_{sub}, is calculated using the expression $E_{sub} = [E_{BP\text{-doped}} + E_{single}(B/P)] - [E_{BP} + E_{single}(C/Si)]$ in terms of the optimized total energies of pristine monolayer BP, E_{BP}; dopant atom, E_C or E_{Si}; doped monolayer BP, $E_{BP\text{-doped}}$; and of the substituted atom, E_B or E_P, all calculated within the same supercell. E_{sub} for a 5 × 5 supercell are 1.05 eV and 0.73 eV for C and Si substitution, respectively. These data indicate that the substitution is endothermic for both types but feasible since the required energy is not very high.

We have also investigated whether local symmetries are preserved for the honeycomb monolayer BP (with a lattice constant of 3.21 Å). The B and P atoms indeed preserve the hexagonal symmetry and planarity with no buckling. However, a major effect of replacing a B atom with C has been shortening of the bond lengths. For instance, the B–B bond length of 1.85 Å in pristine BP decreases to 1.79 Å for C–B bonds. Likewise for P, the C–P distance of 3.17 Å becomes 3.21 Å for B–P. In contrast, substituting Si instead of P has caused a relative repulsion; *e.g.* bond lengths of 3.23 Å and 1.92 Å for Si–P and Si–B, respectively. The B–P bond distance has increased slightly, to 1.85 Å with respect to the original 1.83 Å. These results can be understood simply by comparing atomic radii of the B, C, P and Si atoms: *i.e.* C has a smaller atomic radius than B and Si has a larger atomic radius than the P atom.

Regarding the magnetic states of pure and doped systems of single layer BP, both the former and the latter yield spin unpolarized ground states. This is confirmed by varying supercell sizes.

The electronic band structure of 5 × 5 doped BP is displayed in Fig. 3. The donor state coming from C doping appears below the lowest occupied conduction band, which leads to n-type doping. Obviously, the substitution of B with C causes a substantial shift-down of the valence band minimum. This phenomenon is attributed to the impurity (donor) states which constitute the impurity band. Moreover, there is prominent broadening of the bands, especially at the *K*-point, with respect to pristine BP.

On the other hand, Si doping results in acceptor states close to the top of the valence band. The opening between the VBM and the impurity band is 0.7 eV. It was found that in general, the bands of 5 × 5 BP seem to be slightly more dispersed as compared to the lighter doped counterparts. However, since this dispersion level can be tolerated as the impurity band stands out clearly, 5 × 5 was decided to be a sufficient system size for the use of electrodes in the following transport calculations of the p–n junction of BP.

As evident from the right-hand sides of the band plots in Fig. 3, the charge density of the top valence band (I) is more or less evenly distributed among mostly the P and partially B atoms, which are not the nearest neighbors of the substitutional C. On the other hand, the majority of the charge is localized around the C impurity atom for (II), whereas it starts to scatter among B and P atoms for the bottom-most conduction band. Analogously, for Si doping a similar trend in the evolution of the charge density distribution is observed. While the C atom contributed with its s electrons to the semi-core bands, the orbital characteristics of the top two valence bands are constituted of only p_z states with increased total occupancies due to the extra electron donated by the C atom. As for the donor impurity band, they consist mostly of p_z type orbitals. For Si doping, the Si atom creates acceptor states. The top states of the valence band display p_z characteristics.

Finally, it is worth mentioning the results from a Bader charge analysis of single layer BP. For pristine BP, the total charge is shared among B and P atoms as 2.11 *e* ($B^{+0.89}$) for the former and 5.89 *e* ($P^{-0.89}$) for the latter (naturally summing up to a total of 8 electrons). For n-type doping when C substitutes B, C atoms possess 5.70 *e* ($C^{-1.70}$). While the B atom donates electrons, the C atom accepts electrons from the nearest P atoms, thus resulting in 2.6 *e* local charge difference with respect to the

 This journal is © the Owner Societies 2015

View Article Online

Published on 16 April 2015. Downloaded by Bilkent University on 05/05/2015 13:53:39.

pristine system. In a similar manner, for p-type doping (P substituted by Si), the Si atoms possess 2.20 e ($Si^{+1.80}$) donating its electrons to the nearest B atoms. This leads to 3.7 e local charge difference as compared to the undoped system. The charge localization corresponding to the impurity levels are shown in Fig. 3.

4 Transport properties of the BP based p–n junction

Next, we investigated the performance of a p–n junction based on single layer BP. As mentioned in the previous section, n- and p-type doping of BP were achieved by substituting B with C and P with Si, respectively. The device structures used in transport calculations are shown in Fig. 4. In order to calculate the electron transport across the p–n junction shown in Fig. 4, we partitioned the device into three regions, namely the left electrode, the right electrode, and the scattering region. The electrodes are modelled as semi-infinite. We focused on the high doping case with an impurity concentration of 10^{13} cm^{-2} on both the p- and n-sides. Previously, such large doping concentration was adopted to construct a p–n junction based on single layer MoS_2.[54] As seen in Fig. 4, two different transport directions, namely zigzag and armchair, are possible. Since the doping concentration is identical for both device configurations, the armchair p–n junction has shorter electrode and junction regions whose effects on the electron transport are discussed below.

The transmission coefficient $\langle T(E)\rangle$, which refers to the energy-dependent total probability of electrons to be propagated through a device, averaged over a Brillouin zone perpendicular to the transport direction is defined as: $\langle T(E)\rangle = \mathrm{Tr}[G^{r}\Gamma_{L}(E)G^{a}(E)\Gamma_{R}(E)]$. Here, $G^{r(a)}$ is the retarded (advanced) Green function and $\Gamma_{(L,R)}(E) = i\left(\Sigma^{r}_{L,R} - \Sigma^{a}_{L,R}\right)$ describes the level broadening due to the left and right electrodes expressed in terms of the self energies $\Sigma_{L,R}$ of the electrodes, which express the influence of the electrodes on the scattering region.

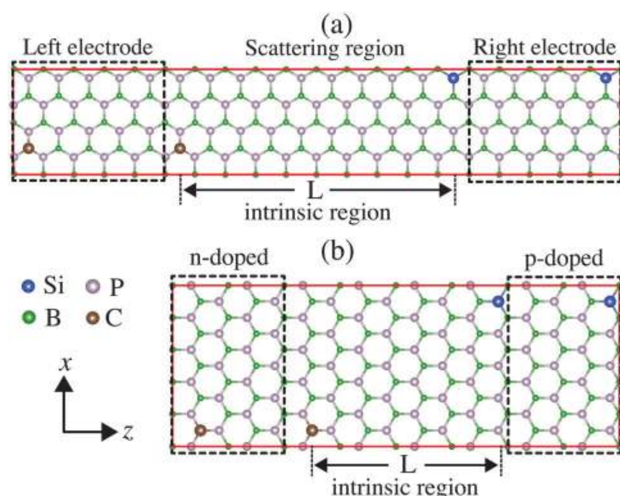

Fig. 4 The device models: for (a) zigzag and (b) armchair p–n junctions.

The current across the p–n junction is calculated using the Landauer–Buttiker formula:

$$I = \frac{2e}{h}\int \langle T(E, V_{\mathrm{bias}})\rangle [f(E-\mu_{L}) - f(E-\mu_{R})]\mathrm{d}E,$$

where $f(E)$ $(1/[\exp(E/kT) + 1])$ is the Fermi distribution function and $\mu_{L/R}$ the chemical potential in the left/right electrode. $V_{\mathrm{bias}} = (\mu_{L} - \mu_{R})/e$ defines the bias window. In order to apply an external bias, the Fermi level of the electrodes is shifted relative to each other and the electronic occupations of the system are determined by the electrochemical potential (*i.e.*, $\mu_{L/R}$) of the electrodes.

The *I–V* curves for both zigzag and armchair terminated p–n junctions are shown in Fig. 5. An initial clear observation is that zigzag and armchair p–n junctions exhibit quite different *I–V* characteristics from each other even when the doping concentrations are the same. Both p–n junctions display a negative differential resistance (NDR) effect between 0 V and 0.6 V in the forward bias, corresponding to a typical Esaki diode behavior.[55] In our device module, there is 1/40 impurity per host atom, resulting in heavy doping. Due to the strong interactions among the impurities, the bands originating from impurity

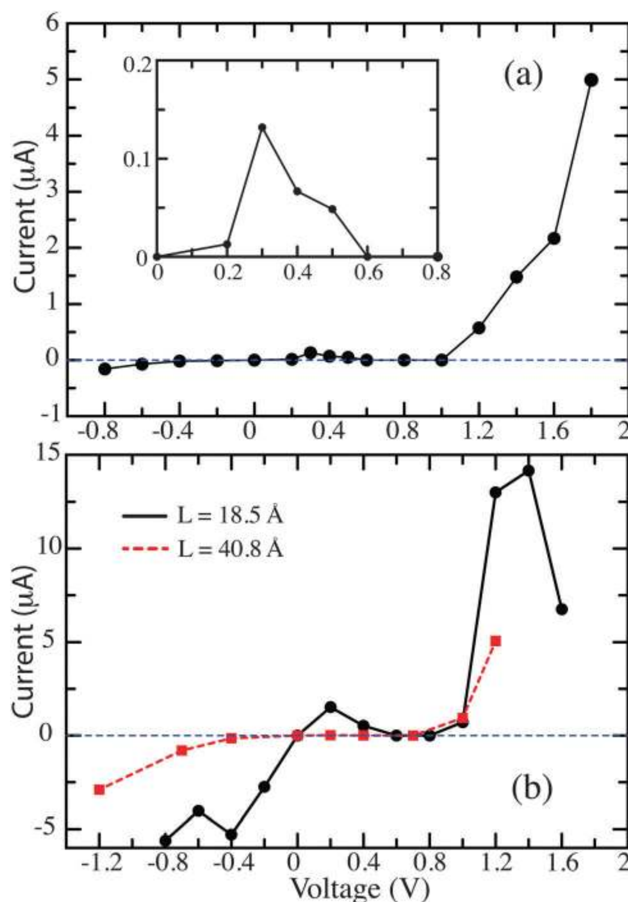

Fig. 5 The calculated current–voltage (*I–V*) curves for (a) zigzag and (b) armchair terminated p–n junctions. The inset in (a) shows *I–V* for *V* = 0–0.8 V. In (b) *I–V* curves for the armchair terminated p–n junction with two different intrinsic region sizes are shown.

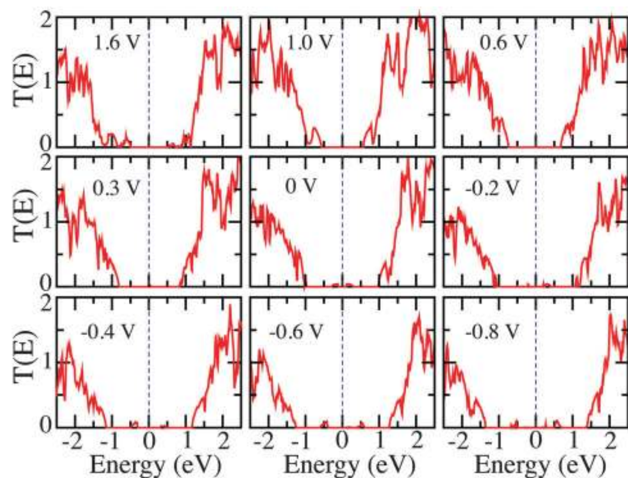

Fig. 6 Transmission spectrum of the zigzag p–n junction for different applied bias.

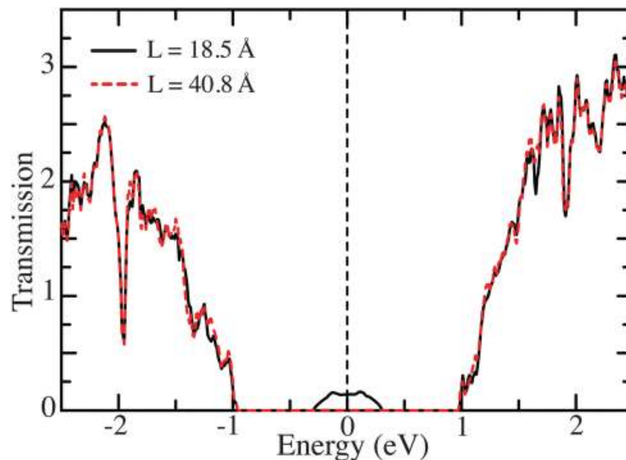

Fig. 7 Zero bias transmission spectrum of the armchair p–n junction for two different intrinsic region lengths (L).

Published on 16 April 2015. Downloaded by Bilkent University on 05/05/2015 13:53:39.

atoms broaden into a band either just below the conduction band or above the valence band edges.

When a small positive bias is applied, electrons from the conduction band of the n-region tunnel into available states in the valence band of the p-region, thereby leading to an increase in the current for $0 < V_{\text{bias}} < 0.6$ V, see the inset in Fig. 5(a). The peak and valley of the current for the zigzag p–n junction are located at $V = 0.3$ V and 0.6 V, respectively. In order to better understand charge transport properties, a variation in the transmission spectrum as a function of applied bias for the zigzag p–n junction is shown in Fig. 6. Since the electrodes are heavily doped, small transmission peaks appear within the transport gap, originating from quantum tunneling of electrons between n and the p sides of the junction. These transmission features play a significant role in the aforementioned NDR. With increasing positive voltage, these small peaks become narrower and lower. For $V_{\text{bias}} < 0.3$ V, the bias window includes these transmission peaks, which leads to an increase in the current. Applying a positive voltage larger than 0.6 V suppresses these small peaks. At 1 V, the transport gap of the electrodes coincides, and the transmission spectrum displays a clear transport gap of 1.0 eV, which is close to the band gap of pristine BP. Beyond this value, the zigzag-terminated p–n junction starts to act like a conventional diode with a large positive rectification. The typical conventional diode behavior over all applied bias range can be achieved by either decreasing the impurity concentration or increasing the length of the intrinsic part in the junction region.[56] In reversed bias, electrons easily tunnel from the valence band of the p-region to the conduction band of the n-region, giving rise to an increase in current for $V_{\text{bias}} > -0.4$ V. The current for negative voltage exhibits no NDR effect. In contrast to the positive bias case, the transmission peaks within the transport gap become larger and contribute to the current with increasing negative voltage.

In Fig. 5(b), we also present I–V curves for armchair terminated p–n junctions having different intrinsic region lengths (L). Here, L is defined as the distance between the impurity atoms at both sides of the junction, *i.e.*, distance between adjacent Si and C atoms in the scattering region. Two different L values (18.5 and 40.8 Å) are considered. In order to clarify the effect of the intrinsic region length, the zero bias transmission spectrum of the armchair p–n junction is shown in Fig. 7 for both L values. For the short intrinsic region, *i.e.*, L = 18.5 Å (implying a quite strong impurity–impurity interaction), it is observed that the transmission peaks originating from impurity states appear around the Fermi level, which are the origins of the NDR for $V_{\text{bias}} < 0.6$ V. For L = 18.5 Å, electrons at the Fermi level easily penetrate the junction region *via* tunneling. In addition to the NDR observed between 0–0.6 V, another NDR with a much larger peak current value appears between 1–1.6 V for L = 18.5 Å. For the first (second) NDR, the peak position of the current is found to be at 0.2 (1.4) V. In reversed bias, due to the heavily doped electrodes and the short intrinsic region length, the current exhibits a negative rectification up to −0.4 V.

However, extending the intrinsic region length to 40.8 Å along the transport direction significantly reduces the transmission around the Fermi level due to the weakening of the interaction between the impurity atoms at the n- and p-sides of the junction thereby leading to a much thicker tunnel barrier for electrons (see Fig. 7). The p–n junction with a longer L has a clear transport gap of 2 eV. The disappearance of small transmission peaks within this transport gap with increasing L certainly translates into a significant modulation in the I–V characteristic. In Fig. 5(b), we also present the I–V curve for the armchair p–n junction for L = 40.8 Å. It is evident that the I–V characteristic resembles a diode like behavior as the size of the intrinsic region is increased. While the p–n junction with a short L exhibits an NDR and negative rectification, increasing the length of the intrinsic region weakens the NDR and results in a very small current for $V_{\text{bias}} < 1$ V.

5 Conclusions

We investigated the electronic, vibrational, mechanical and transport properties of 2D single layer BP and the effects of

Published on 16 April 2015. Downloaded by Bilkent University on 05/05/2015 13:53:39.

p- and n-type doping in order to develop an understanding for the optimum design of a potential monolayer p–n junction. Our results indicate that due to its mechanical stability and promising electronic properties, h-BP would be a promising candidate for application in a p–n junction. From the above analysis, we conclude that the device characteristics of p- and n-type doped BP are suitable for a functional 2D p–n junction at the nanoscale. Furthermore, electron transport through this junction can be modified by altering the length of the intrinsic region *via* modifying the electron tunneling between the n and p regions. We also achieved distinct device characteristics, including NDR and conventional rectifying diode behavior. Our findings provide detailed insight into the realization of layered BP based nanoelectronic devices.

Acknowledgements

This work was supported by the Flemish Science Foundation (FWO-Vl), the Methusalem foundation of the Flemish government and the Bilateral program FWO-TUBITAK (under the Project No. 113T050) between Flanders and Turkey. Computational resources were provided by TUBITAK ULAKBIM, High Performance and Grid Computing Center (TR-Grid e-Infrastructure), and HPC infrastructure of the University of Antwerp (CalcUA) a division of the Flemish Supercomputer Center (VSC), which is funded by the Hercules foundation. D.C. is supported by a FWO Pegasus-short Marie Curie Fellowship. H.S. is supported by a FWO Pegasus Marie Curie-long Fellowship. E.D. acknowledges support from Bilim Akademisi – The Science Academy, Turkey under the BAGEP program.

References

1 K. Novoselov, A. Geim, S. Morozov, D. Jiang, M. Katsnelson, I. Grigorieva, S. Dubonos and A. Firsov, *Nature*, 2005, **438**, 197.
2 K. Novoselov, A. Geim, S. Morozov, D. Jiang, Y. Zhang, S. Dubonos, I. Grigorieva and A. Firsov, *Science*, 2004, **306**, 666.
3 A. K. Geim, *Science*, 2009, **324**, 1530.
4 A. Castro Neto, F. Guinea, N. Peres, K. Novoselov and A. Geim, *Rev. Mod. Phys.*, 2009, **81**, 109.
5 K. K. Kim, A. Hsu, X. Jia, S. M. Kim, Y. Shi, M. Hofmann, D. Nezich, J. F. Rodriguez-Nieva, M. Dresselhaus, T. Palacios and J. Kong, *Nano Lett.*, 2012, **12**, 161.
6 Y. Shi, C. Hamsen, X. Jia, K. K. Kim, A. Reina, M. Hofmann, A. L. Hsu, K. Zhang, H. Li, Z.-Y. Juang, M. S. Dresselhaus, L.-J. Li and J. Kong, *Nano Lett.*, 2010, **10**, 4134.
7 B. Wang and M.-L. Bocquet, *J. Phys. Chem. Lett.*, 2011, **2**, 2341.
8 K. H. Lee, H.-J. Shin, J. Lee, I.-y. Lee, G.-H. Kim, J.-Y. Choi and S.-W. Kim, *Nano Lett.*, 2012, **12**, 714.
9 X. Li, J. Yin, J. Zhou and W. Guo, *Nanotechnology*, 2014, **25**, 105701.
10 Z. Liu, Y. Gong, W. Zhou, L. Ma, J. Yu, J. C. Idrobo, J. Jung, A. H. MacDonald, R. Vajtai, J. Lou and P. M. Ajayan, *Nat. Commun.*, 2013, **4**, year.
11 K. Watanabe, T. Taniguchi and H. Kanda, *Nat. Mater.*, 2004, **3**, 404.
12 B. Wang and M.-L. Bocquet, *J. Phys. Chem. Lett.*, 2011, **2**, 2341.
13 M. Gao, A. Lyalin and T. Taketsugu, *Catalysts*, 2011, **1**, 18.
14 O. Lehtinen, E. Dumur, J. Kotakoski, A. V. Krasheninnikov, K. Nordlund and J. Keinonen, *Nucl. Instrum. Methods Phys. Res., Sect. B*, 2011, **269**, 1327.
15 M. S. Si and D. S. Xue, *J. Phys. Chem. Solids*, 2010, **71**, 1221.
16 M. Corso, W. Auwrter, M. Muntwiler, A. Tamai, T. Greber and J. Osterwalder, *Science*, 2004, **303**, 217.
17 M. S. Si, J. Y. Li, H. G. Shi, X. N. Niu and D. S. Xue, *Europhys. Lett.*, 2009, **86**, 46002.
18 Y. Chen, H. Wang, H. Wang, J. X. Zhao, Q. H. Cai, X.-G. Wang and Y. H. Ding, *Appl. Surf. Sci.*, 2013, **273**, 293.
19 H. Park, A. Wadehra, J. W. Wilkins and A. H. Castro Neto, *Appl. Phys. Lett.*, 2012, **100**, 253115.
20 P. Popper and T. Inhles, *Nature*, 1957, **179**, 1075.
21 P. Kocinski and M. Zbroszczyk, *Semicond. Sci. Technol.*, 1995, **10**, 1452.
22 Y. Gu, H. Zheng, F. Guo, Y. Qian and Z. Yang, *Chem. Lett.*, 2002, 724.
23 E. Schroten, A. Goossens and J. Schoonman, *J. Electrochem. Soc.*, 1999, **146**, 2045.
24 S. Z. Sayyad-Alangi, M. T. Baei and S. Hashemian, *J. Sulfur Chem.*, 2013, **34**, 407.
25 S. Z. Sayyad-Alangi, S. Hashemian and M. T. Baei, *Phosphorus, Sulfur Silicon Relat. Elem.*, 2014, **189**, 453.
26 M. T. Baei, A. A. Peyghan and M. Moghimi, *Monatsh. Chem.*, 2012, **143**, 1627.
27 H. Sahin, S. Cahangirov, M. Topsakal, E. Bekaroglu, E. Akturk, R. Senger and S. Ciraci, *Phys. Rev. B: Condens. Matter Mater. Phys.*, 2009, **80**, 155453.
28 J. Dong, H. Li and L. Li, *NPG Asia Mater.*, 2013, **5**, e56.
29 P. Tsipas, S. Kassavetis, D. Tsoutsou, E. Xenogiannopoulou, E. Golias, S. A. Giamini, C. Grazianetti, D. Chiappe, A. Molle, M. Fanciulli and A. Dimoulas, *Appl. Phys. Lett.*, 2013, **103**, 251605.
30 C. Tusche, H. Meyerheim and J. Kirschner, *Phys. Rev. Lett.*, 2007, **99**, 026102.
31 G. Kresse and J. Hafner, *Phys. Rev. B: Condens. Matter Mater. Phys.*, 1993, **47**, 558.
32 G. Kresse and J. Furthmüller, *Phys. Rev. B: Condens. Matter Mater. Phys.*, 1996, **54**, 11169.
33 P. E. Blöchl, *Phys. Rev. B: Condens. Matter Mater. Phys.*, 1994, **50**, 17953.
34 J. P. Perdew, K. Burke and M. Ernzerhof, *Phys. Rev. Lett.*, 1996, **77**, 3865.
35 J. Paier, M. Marsman, K. Hummer, G. Kresse, I. C. Gerber and J. G. Ángyán, *J. Chem. Phys.*, 2006, **124**, 154709.
36 B. G. Janesko, T. M. Henderson and G. E. Scuseria, *Phys. Chem. Chem. Phys.*, 2009, **11**, 443–454.
37 A. V. Krukau, O. A. Vydrov, A. F. Izmaylov and G. E. Scuseria, *J. Chem. Phys.*, 2006, **125**, 224106.

View Article Online

38 G. H. F. Diercksen, B. O. Roos and A. J. Sadlej, *Int. J. Quantum Chem.*, 1983, **24**, 265.
39 D. Alfè, *Comput. Phys. Commun.*, 2009, **180**, 2622–2633.
40 M. Brandbyge, J.-L. Mozos, P. Ordejón, J. Taylor and K. Stokbro, *Phys. Rev. B: Condens. Matter Mater. Phys.*, 2002, **65**, 165401.
41 J. M. Soler, E. Artacho, J. D. Gale, A. Garca, J. Junquera, P. Ordejón and D. Sánchez-Portal, *J. Phys.: Condens. Matter*, 2002, **14**, 2745.
42 N. Troullier and J. Martins, *Phys. Rev. B: Condens. Matter Mater. Phys.*, 1991, **43**, 1993.
43 D. Çakır, F. M. Peeters and C. Sevik, *Appl. Phys. Lett.*, 2014, **104**, 203110.
44 R. J. Archer, R. Y. Koyama, E. E. Loebner and R. C. Lucas, *Phys. Rev. Lett.*, 1964, **12**, 538–540.
45 J. I. Ejembi, I. H. Nwigboji, L. Franklin, Y. Malozovsky, G. L. Zhao and D. Bagayoko, *J. Appl. Phys.*, 2014, **116**, 103711.
46 M. Topsakal, E. Aktürk and S. Ciraci, *Phys. Rev. B: Condens. Matter Mater. Phys.*, 2009, **79**, 115442.
47 A. Zaoui and F. E. H. Hassan, *J. Phys.: Condens. Matter*, 2001, **13**, 253.
48 T. Udagawa, *P–n junction type boron phosphide-based semiconductor light-emitting device and production method thereof*, *US Pat.*, 6,831,304, 2004.
49 Y.-N. Xu and W. Ching, *Phys. Rev. B: Condens. Matter Mater. Phys.*, 1991, **44**, 7787.
50 X. Cao, B. Clubine, J. Edgar, J. Lin and H. Jiang, *Appl. Phys. Lett.*, 2013, **103**, 191106.
51 H. Peelaers and C. G. Van de Walle, *Phys. Rev. B: Condens. Matter Mater. Phys.*, 2012, **86**, 241401.
52 T. Low, A. Rodin, A. Carvalho, Y. Jiang, H. Wang, F. Xia and A. C. Neto, *Phys. Rev. B: Condens. Matter Mater. Phys.*, 2014, **90**, 075434.
53 Here, C and Si doping should only be considered as prototype model. To realize the n- and p-type doping, good selective substitution is required.
54 Q.-Q. Sun, Y.-J. Li, J.-L. He, W. Yang, P. Zhou, H.-L. Lu, S.-J. Ding and D. W. Zhang, *Appl. Phys. Lett.*, 2013, **102**, 093104.
55 L. Esaki, *IEEE Trans. Electron Devices*, 1976, **23**, 644.
56 Z. Li, J. Zheng, Z. Ni, R. Quhe, Y. Wang, Z. Gao and J. Lu, *Nanoscale*, 2013, **5**, 6999.

Published on 16 April 2015. Downloaded by Bilkent University on 05/05/2015 13:53:39.

This journal is © the Owner Societies 2015